Pergamon

Int. J. Heat Mass Transfer. Vol. 37, No. 16, pp. 2391–2398, 1994

0017-9310/94 $7.00 + 0.00

0017-9310(94)E0081-5

# Transient heat transfer through an insulation slab with simultaneous moisture redistribution

N. E. WIJEYSUNDERA† and S. J. WILSON‡

†Department of Mechanical and Production Engineering, and
‡Department of Mathematics, National University of Singapore,
10 Kent Ridge Crescent, Singapore 0511

(*Received* 7 *September* 1993 *and in final form* 11 *March* 1994)

**Abstract** The accuracy of three models for the interpretation of moisture redistribution experiments with fiber glass slabs is investigated. The initial quasi-steady state of the evaporation–condensation process is well predicted by all three models. The quasi-steady model and the numerical model predict much faster changes in the heat flux and temperature distribution during the final drying–redistribution process. The semi-empirical model which incorporates the 'falling rate' evaporation period gives more accurate predictions of the experimental data. This model is used to obtain additional physical information on the moisture redistribution and drying process in the slab.

## INTRODUCTION

THE TRANSFER of heat and moisture in porous building materials has been a topic of considerable research interest in the recent past. This is mainly due to the widespread use of porous materials such as fiber glass in building and HVAC applications. Moisture infiltration into insulations usually results in condensation of water. Subsequent changes in the operating conditions of the moisture-laden insulation system will lead to a redistribution of moisture due to evaporation–condensation processes. These processes are usually accompanied by additional energy transfer. From the point of view of energy conservation and insulation system design, it is important to understand and quantify the aforementioned heat and moisture transport processes.

Early work on the influence of moisture on the heat transfer through building materials was done by Bomberg and Shirtliffe [1]. Langlais and Klarsfeld [2] investigated the moisture redistribution process in an insulation slab that was sprayed with water before placing it in a heat-flow meter apparatus. Thomas *et al.* [3] performed similar experiments over a wide range of conditions. Kumaran [4, 5] measured the heat flux during the moisture redistribution process in fiber glass slabs. Wijeysundera *et al.* [6] compared their measurements with calculations for the initial quasi-steady phase of the moisture redistribution in fiber glass insulation slabs. The effective thermal conductivity of insulations in the presence of moisture transfer was measured by Crausse *et al.* [7].

Analytical models for the moisture and heat transfer through porous insulations were presented by Ogniewicz and Tien [8] and Motakef and El-Masri [9]. Both papers dealt with the quasi-steady phase of the moisture transfer process. Shapiro and Motakef [10] included the unsteady movement of the liquid front and condensation in a porous slab.

Vafai and co-workers [11–13] have performed detailed numerical studies of the moisture transfer in insulations for several different boundary conditions. The effects of infiltration on the performance of insulations was simulated by Tien and Vafai [14, 15]. Tao *et al.* [16] presented a numerical study of condensation in insulations, including frosting effects.

Most of the experimental results reported in the recent literature [2–6] for moisture redistribution in an insulation are for a situation where the insulation slab was sprayed with a known quantity of water before placing it in a heat-flow meter apparatus. Comparison of the results of such experiments with numerical computations was reported by Kumaran and Mitalas [17] and Hokoi and Kumaran [18]. In the latter paper a parameter fitting procedure was used to interpret the experimental data.

The objectives of the present study are: (a) to compare the accuracy of three models for the interpretation of moisture redistribution experiments and (b) to use the models to obtain physical information on the transient moisture and heat transfer processes in an insulation slab.

The next section of the paper gives a brief review of the experiments and the development of the physical model. Subsequent sections will present the results of the computations and the conclusions.

## REVIEW OF EXPERIMENTS

Figure 1 shows schematically the conditions of the moisture redistribution experiments that have been

## NOMENCLATURE

| | |
|---|---|
| $A$ | constant in equation (4) [K] |
| $a(T)$ | coefficient in equation (10) [J K$^{-1}$ m$^{-1}$] |
| $B$ | constant in equation (4) |
| $b(T)$ | coefficient in equation (10) [W m$^{-1}$ K$^{-1}$] |
| $C(z, t)$ | vapor concentration [kg (kg dry air)$^{-1}$] |
| $c_a$ | specific heat capacity of air [J kg$^{-1}$ K$^{-1}$] |
| $c_s$ | specific heat capacity of solid [J kg$^{-1}$ K$^{-1}$] |
| $c_w$ | specific heat capacity of water [J kg$^{-1}$ K$^{-1}$] |
| $D$ | vapor diffusivity [m s$^{-1}$] |
| $D_0$ | vapor diffusivity in QS model |
| $g(T)$ | Clausius–Clapeyron relation |
| $g'(T)$ | $dg/dT$ |
| $H_{fg}$ | latent heat of vaporization [J kg$^{-1}$] |
| $k_a$ | thermal conductivity of air [W m$^{-1}$ K$^{-1}$] |
| $k_s$ | thermal conductivity of solid [W m$^{-1}$ K$^{-1}$] |
| $k_w$ | thermal conductivity of water [W m$^{-1}$ K$^{-1}$] |
| $k_0$ | thermal conductivity in QS model [W m$^{-1}$ K$^{-1}$] |
| $L$ | thickness of slab [m] |
| $M$ | mass of water sprayed [kg m$^{-2}$] |
| $q$ | heat flux [W m$^{-2}$] |
| $q_0$ | heat flux during quasi-steady period [W m$^{-2}$] |
| $R_{hf}$ | thermal resistance of the heat-flux-meter [K m$^2$ W$^{-1}$] |
| $T(z, t)$ | temperature distribution [K] |
| $T_1$ | temperature of hot face [K] |
| $T_2$ | temperature of cold face [K] |
| $T_m$ | mean temperature of slab [K] |
| $T_3$ | temperature at the drying front [K] |
| $T_w(z)$ | temperature in the wet region [K] |
| $t$ | time [s] |
| $W(t)$ | mass of liquid in wetted surface [kg m$^{-2}$] |
| $W_0$ | mass of water in wetted surface at beginning of falling rate period [kg m$^{-2}$] |
| $x$ | position of drying front [m] |
| $z$ | coordinate along slab [m]. |

Greek symbols

| | |
|---|---|
| $\Gamma(z, t)$ | condensation rate [kg m$^{-3}$] |
| $\varepsilon$ | void fraction of dry slab |
| $\theta$ | liquid saturation [kg [kg (max)]$^{-1}$] |
| $\lambda$ | decay parameter in equation (17) [s$^{-1}$] |
| $\rho_a$ | density of air [kg m$^{-3}$] |
| $\rho_w$ | density of water [kg m$^{-3}$] |
| $\rho_s$ | density of dry solid [kg m$^{-3}$] |
| $\tau$ | tortuousity |
| $\tau_s$ | quasi-steady period [s] |
| $\Phi$ | vapor flux, [kg m$^{-2}$ s$^{-1}$] |
| $\Phi_0$ | vapor flux at $z = 0$ [kg m$^{-2}$ s$^{-1}$]. |

reported by several investigators [2–6]. In these experiments a few layers of fiber glass were assembled to form a slab of insulation. Water was sprayed on one face of the slab before being sealed in a plastic bag to prevent further exchange of moisture with the surroundings. The sealed insulation slab was placed in a heat-flow-meter apparatus with the moisture-laden face bearing against the hot plate of the apparatus. Heat-flux-meters at the hot and cold faces are used to measure the heat flux variation. In the experiments reported by Wijeysundera *et al.* [6], thermocouples were located at the interfaces of the insulation layers to measure the variation of the temperature distribution in the slab during the moisture redistribution process. In addition, the moisture distribution in the slab was measured by weighing the layers at different times. The details pertaining to these experiments are also available in ref. [19].

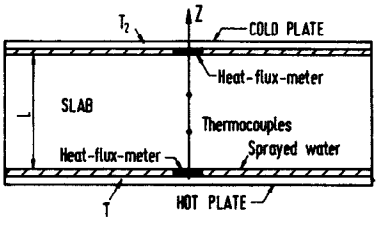


FIG. 1. Physical situation in the moisture redistribution experiment.

Figure 3(a) shows a typical measured variation of the heat flux. It is seen that the heat flux reaches a quasi-steady value following a short initial transient. At the end of this period, the flux decreases gradually until it attains a final steady value close to that obtained with a dry slab under the same conditions of temperature. The measured variation of the mass of water in the insulation layer bearing against the hot plate is shown in Fig. 2. At the end of the final transient period, all the water is deposited in the insulation layer adjacent to the cold plate, while the rest of the slab is practically dry [6, 19].

From the aforementioned experimental observations the following physical processes may be identified. At the hot face of the insulation, water evap-

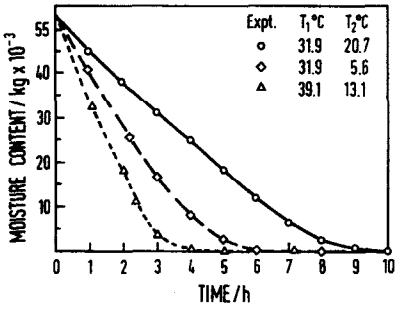


FIG. 2. Variation of total moisture content in the insulation layer with time.

orates and the vapor produced diffuses towards the cold face. Some of this vapor condenses in the body of the slab, while the vapor reaching the cold face condenses at this point and the resulting water is deposited in the insulation layer adjacent to the cold plate. When most of the water at the hot face has evaporated, that insulation layer begins to dry out. This creates a 'drying front' in the insulation slab which moves across the slab until all the water in the body of the slab has evaporated. This transient period constitutes the 'drying–redeposition' phase of the moisture transfer process.

## PHYSICAL MODEL

Several assumptions are made in developing the physical model to simulate the transient heat and moisture transfer processes described above. These

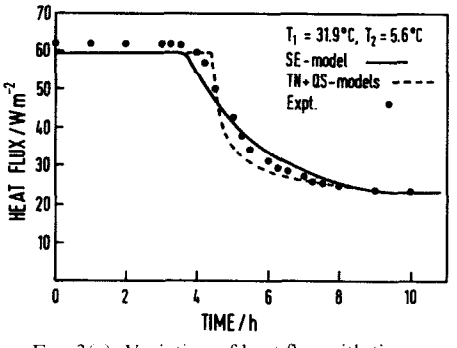


FIG. 3(a). Variation of heat flux with time.

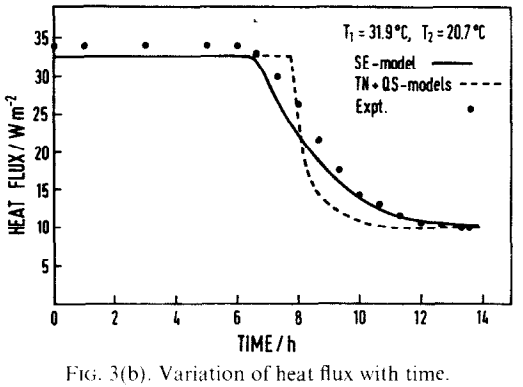


FIG. 3(b). Variation of heat flux with time.

are: (a) the total gas phase pressure is constant; (b) the insulation material is homogeneous; (c) the liquid is in a pendular state due to the relatively low liquid content; and (d) there are no convective contributions to the heat and mass transfer.

Subject to the above assumptions, the governing equations of mass and energy can be written as follows:

For vapor diffusion,

$$\rho_a \frac{\partial C}{\partial t} = \frac{\partial}{\partial z}\left[\rho_a D \frac{\partial C}{\partial z}\right] - \Gamma. \tag{1}$$

For liquid transfer,

$$\varepsilon \rho_w \frac{\partial \theta}{\partial t} = \Gamma. \tag{2}$$

For energy transfer,

$$(\rho c)_e \frac{\partial T}{\partial t} = \frac{\partial}{\partial z}\left[k_e \frac{\partial T}{\partial z}\right] + \Gamma H_{fg}. \tag{3}$$

The meaning of the symbols is defined in the Nomenclature. In the region of the slab where condensation or evaporation occurs, the vapour concentration is a function of the local temperature, which is given by the Clausius–Clapeyron relation:

$$C(T) = g(T) = B\exp\left[A\left(\frac{1}{T_0} - \frac{1}{T}\right)\right]. \tag{4}$$

The values of the constants $A$, $B$ and $T_0$ are given in Table 1. In the wet region of the slab, the physical properties are dependent on the local liquid saturation. The properties may be expressed in the following form [11–13]:

$$(\rho c)_e = (1-\varepsilon)\rho_s c_s + \varepsilon\rho_w c_w \theta + \varepsilon(1-\theta)\rho_a c_a$$
$$k_e = (1-\varepsilon)k_s + \varepsilon\theta k_w + \varepsilon(1-\theta)k_a. \tag{5}$$

The vapor diffusion coefficient is obtained from the empirical equation [20]:

$$D = \frac{\varepsilon(1-\theta)}{\tau} \times 1.97 \times 10^{-5}\left[\frac{T_m}{255.2}\right]^{1.685}. \tag{6}$$

Since the quantity of water sprayed on the insulation face is small, the initial thickness of the wet region is estimated to be less than about a millimeter. Therefore, it can be treated as a plane source of moisture from which evaporation occurs.

The other boundary conditions are:

$$\text{at } z = 0 \quad T(z) = T_1 \quad \text{and}$$
$$\text{at } z = L \quad T(z) = T_2. \tag{7}$$

For dry regions of the insulation slab, the condensation (or evaporation) rate $\Gamma$ is zero. In the wet region, $\Gamma$ can be eliminated from equations (1) and (3) by using equation (4) to relate the concentration $C$ to the local temperature $T$. This gives the combined energy equation as

Table 1. Physical properties and other data

| | | |
|---|---|---|
| $L = 0.04$ m | $\varepsilon = 0.98$ | $\tau = 1.0$ |
| $T_0 = 301$ K | $c_s = 840$ J kg$^{-1}$ K$^{-1}$ | $H_{fg} = 2442 \times 10^3$ J kg$^{-1}$ |
| $B = 0.0232$ | $c_w = 4200$ J kg$^{-1}$ K$^{-1}$ | $\rho_0 = 53$ kg m$^{-3}$ |
| $A = 5271.2$ K | $c_a = 1010$ J kg$^{-1}$ K$^{-1}$ | $k_0 = 0.036$ W m$^{-1}$ K$^{-1}$ |
| $k_s = 0.750$ W m$^{-1}$ K$^{-1}$ | $\rho_s = 2650$ kg m$^{-3}$ | $R_{hf} = 0.015$ K m$^{-1}$ W$^{-1}$ |
| $k_w = 0.610$ W m$^{-1}$ K$^{-1}$ | $\rho_w = 997$ kg m$^{-3}$ | |
| $k_a = 0.022$ W m$^{-1}$ K$^{-1}$ | $\rho_a = 1.2$ kg m$^{-3}$ | |

$$\left[(\rho c)_e + \rho_a g'(T) H_{fg}\right]\frac{\partial T}{\partial t} = \frac{\partial}{\partial z}\left[(k_e + \rho_a D g'(T) H_{fg})\frac{\partial T}{\partial z}\right]. \quad (8)$$

Following a similar procedure for equations (1) and (2), the combined moisture transfer equation is obtained as

$$\rho_w \varepsilon \frac{\partial \theta}{\partial t} = \frac{\partial}{\partial z}\left[\rho_a D g'(T)\frac{\partial T}{\partial z}\right] - \rho_a g'(T)\frac{\partial T}{\partial t}. \quad (9)$$

The governing equation for the temperature distribution can be written in the general form

$$a(T)\frac{\partial T}{\partial t} = \frac{\partial}{\partial z}\left[b(T)\frac{\partial T}{\partial z}\right]. \quad (10)$$

In the dry region,

$$a(T) = (1-\varepsilon)\rho_s c_s + \varepsilon \rho_a c_a$$
$$b(T) = (1-\varepsilon)k_s + \varepsilon k_a. \quad (11)$$

In the wet region,

$$a(T) = (\rho c)_e + \rho_a g'(T) H_{fg}$$
$$b(T) = k_e + \rho_a D H_{fg} g'(T). \quad (12)$$

The boundary condition at the wet–dry interface is given by

$$-k_e \left.\frac{dT}{dz}\right|_d - H_{fg}\rho_a D \left.\frac{dC}{dz}\right|_d = -b(T)\left.\frac{dT}{dz}\right|_w. \quad (13)$$

The local condensation (evaporation) rate is given by

$$\Gamma(z, t) = \frac{\partial}{\partial z}\left[\rho_a D g'(T)\frac{\partial T}{\partial z}\right] - \rho_a g'(T)\frac{\partial T}{\partial t}. \quad (14)$$

The local liquid content is obtained from equation (9). The presence of two heat-flowmeters at the two faces of the insulation slab leads to a small temperature difference between the heat sink plates that are maintained at constant temperatures and the faces of the slab. This effect was included by modeling the heat-flux-meters as separate regions with thermal resistances of 0.015 m$^2$ K W$^{-1}$.

Three models are considered for the analysis of the moisture redistribution experiments. These are: (i) the quasi-steady model (QS), (ii) the transient numerical model (TN) and (iii) the semi-empirical model (SE).

*Quasi-steady model*

Some details of the QS model are available in ref. [6]. The main assumption in this model is that the energy transfer and vapor diffusion processes are quasi-steady in relation to the liquid transfer process. Therefore, the transient term in equation (10) is set to zero. It is solved analytically using constant physical properties to obtain the temperature distribution in the wet and dry regions. The condensation (or evaporation) rate is obtained by substituting for $T$ in equation (14) and the liquid content at any time is given by equation (2). The expressions for the various physical quantities are derived in the Appendix.

If the quantity of water sprayed on the surface is $M$ per unit area, then the quasi-steady phase will last for a time given by

$$\tau_s = \frac{M}{\Phi}, \quad (15)$$

where $\Phi$ is the vapor flux at the warm surface during the quasi-steady period.

At the end of this period a drying front starts at the warm surface and it moves towards the cold surface. The water that was condensed during the period $\tau_s$ re-evaporates as the drying front sweeps across the slab. Finally, when it reaches the cold surface all the water will be there.

When the drying front has reached a distance $x$ from the hot face, the heat flux, temperature distribution and condensation rate are obtained from expressions given in the Appendix.

*Transient numerical model*

In the TN model equation (10) is discretized using the control volume approach [21] and the resulting finite difference equations are solved using a fully-implicit scheme. The non-linearity introduced by the dependence of $a(T)$ and $b(T)$ on the temperature is accounted for by using the iterative procedure given by Patankar [21].

The variation of the water content per unit area at the hot face of the slab is given by

$$\frac{dW}{dt} = \rho_a D \left.\frac{\partial C}{\partial z}\right|_{z=0}. \quad (16)$$

When $W = 0$, a drying front is formed at the hot face which propagates towards the cold face. During the solution of the drying phase, the coefficients $a(T)$ and

$b(T)$ of equation (10) are computed according to the position of the moving front, using relations (11) and (12) for the dry and wet nodes, respectively.

Once the temperature distribution at any time is computed, the numerical form of equation (9) is used to obtain the liquid content at each node. Following Vafai *et al.* [11, 12], a node is considered to be dry when its liquid content falls below $10^{-5}$. The computation is carried out until the drying front reaches the cold face of the slab.

*Semi-empirical model*

The development of the SE model was prompted by observation of the measured moisture content variation curves shown in Fig. 2. These curves give the variation of the mass of moisture in the insulation layer adjacent to the warm surface with time. It is interesting to note that until the moisture content reaches about 25% of the original saturated value, its variation with time is approximately linear. This implies a nearly constant evaporation rate at the hot surface. However, as the moisture content falls below a critical value, which is about 25% in the present situation, the evaporation rate decreases with time. This is presumably due to the appearance of dry patches in the wet surface. Such behavior is well known in drying applications [22–25], where a falling rate of drying follows the initial constant rate period. A similar phenomenon is probably responsible for the change in shape of the curves in Fig. 2 because there is an effective drying process occurring at the hot surface of the insulation layer.

There is very little analytical data available on the falling rate period of drying [23]. In the present model it was decided to use the experimental curves of Fig. 2 to obtain fitted data on the variation of the evaporation rate during the falling rate period. A similar approach was used by Plumb *et al.* [24] in modeling drying processes in wood. In convective drying at a surface, the appearance of dry patches reduces the effective area. Wong and Wang [25] have assumed the effective area to be proportional to the moisture content at the surface.

Experimental data in Fig. 2 indicate that during the falling period the variation of the evaporation rate is approximately proportional to the moisture content at the hot surface. Therefore,

$$\frac{dW}{dt} = -\lambda W, \tag{17}$$

where $\lambda$ is a constant to be obtained by fitting the data. The solution of (17) is given by

$$W(t) = W_0 \exp(-\lambda t), \tag{18}$$

where $W_0$ is the moisture content at the start of the falling rate period.

The vapor flux entering the warm face of the insulation is

Table 2. Parameters for the semi-empirical model

| $T_1$ (°C) | $T_2$ (°C) | $\lambda \times 10^4$ ($s^{-1}$) | $W_0$ (kg $m^{-2}$) |
|---|---|---|---|
| 31.9 | 5.6 | 2.40 | 0.086 |
| 31.9 | 20.7 | 1.67 | 0.070 |
| 39.1 | 13.1 | 5.18 | 0.052 |

$$\Phi_0 = -\frac{dW}{dt}. \tag{19}$$

This may be written as

$$\Phi_0 = \lambda W. \tag{20}$$

For each experimental curve shown in Fig. 2, the quantity $\ln [W/W_0]$ is plotted against $t$ and the slope of the line gives the parameter $\lambda$. These values are given in Table 2. Due to the limited range of experimental data available, it was not possible to obtain a general equation for $\lambda$ and $W_0$ in terms of the physical properties of the material and the operating conditions, such as the temperatures of the hot and cold faces.

The numerical procedure to solve equations (10) is similar to that described earlier for the TN model. However, the boundary conditions at the hot surface are now assumed to have the following form:

$$\text{at } x = 0 \text{ and } W \geqslant W_0: \quad \Phi_0 = -\rho_a D g'(T) \left.\frac{\partial T}{\partial z}\right|_0 \tag{21}$$

$$W < W_0; \quad \Phi_0 = \lambda W_0 \exp(-\lambda t). \tag{22}$$

Following Chen and Pei [22], in the dry region the left hand side of (1) is neglected during the falling rate period to obtain the vapor flux in the dry region as

$$\rho_a D \frac{\partial C}{\partial z} = -\Phi_0. \tag{23}$$

The total energy balance at the wet–dry boundary is given by equation (13).

The main difference between the TN model and the SE model is that the latter incorporates a falling rate of evaporation at the hot face, while the former uses the boundary condition given by equation (16), which assumes the evaporation rate to be independent of the moisture level at the hot face.

## RESULTS AND DISCUSSION

The three models described above were used to simulate a series of moisture redistribution experiments, the details of which were reviewed earlier in the paper. The physical properties and other data used in the computations are listed in Table 1.

A comparison of the measured and computed heat flux variation with time is shown in Figs. 3(a) and (b). All three models predict the initial quasi-steady variation of the heat flux well. The above figures show

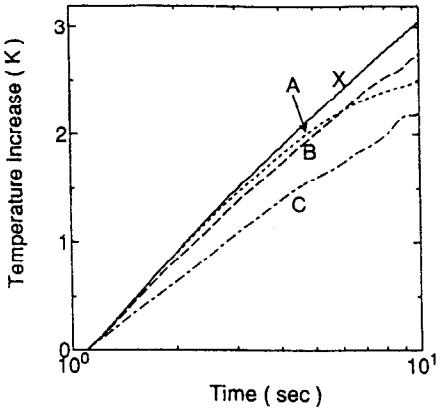


FIG. 4. Variation of heat flux with time for slabs with different initial moisture contents.

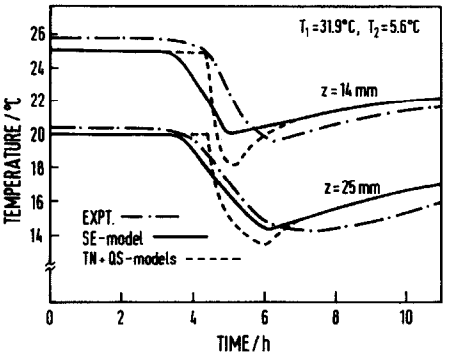


FIG. 5(a). Variation of the temperature at two locations with time.

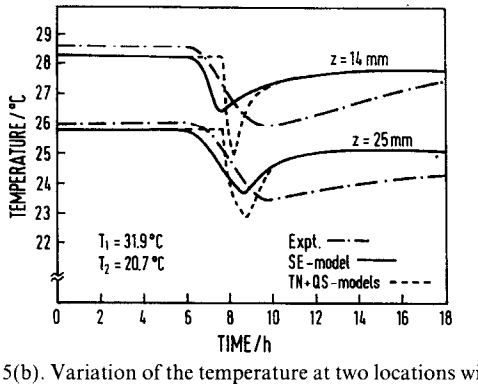


FIG. 5(b). Variation of the temperature at two locations with time.

that as the dry-out commences at the hot face of the insulation, the heat flux begins to decrease. It progressively decreases during the drying period before reaching the final steady value. There was a small difference between the predictions of the QS model and the TN model, but this is well within the accuracy of plotting the curves. There is considerable disagreement between the predictions of the QS model, the TN model and the experiment data during the drying phase. The above models predict a very rapid decrease in the heat flux after the onset of dry-out at the hot face. The predictions of the SE model agree well with the measurements. It should be noted that this model uses two parameters, $\lambda$ and $W_0$, that are 'extracted' from the experimental data shown in Fig. 2. Therefore, the predictions of the SE model cannot be considered to be completely independent. Nevertheless, it does confirm that the slower decrease of the heat flux is probably due to the reduction in the rate of evaporation at the hot face when the liquid content falls below about 25% of the saturation value.

Hokoi and Kumaran [18] used a numerical model to predict the heat flux for moisture redistribution experiments. Their predicted heat flux also showed a sharp drop during the drying phase. This was attributed to a hysteresis effect.

Figure 4 shows a comparison of the measured and computed heat flux variation for an insulation slab with different initial moisture levels at the hot face under the same conditions of temperature. The SE model was used in the computation. The same empirical parameters $\lambda$ and $W_0$, determined earlier from Fig. 2 for one moisture level, were applied during the drying phase. Since the model gives good predictions of the experimental data, the parameters may be considered to be independent of the initial moisture level.

The variation of the temperature history at two points in the slab are shown in Figs. 5(a) and (b). The temperature remains nearly constant during the initial quasi-steady period. As the hot face begins to dry out the temperature within the slab tends to decrease progressively. As the drying front passes a point in the slab, the local temperature attains a minimum and recovers thereafter.

The general physical characteristics of the measured temperature variation is predicted by all three models, as seen in Figs. 5(a) and (b). However, the trend-wise agreement with experimental results is better for the SE model during the drying phase. As before, the QS model and the TN model show steeper reductions in temperature following the onset of drying at the hot face. One of the difficulties with this comparison is the experimental determination of the exact position of the thermocouples. Due to the soft nature of the fiber glass there can be an uncertainty of about 2 mm in the position of the thermocouples [6].

Figure 6 shows a plot of the computed position of the drying front at different times after the com-

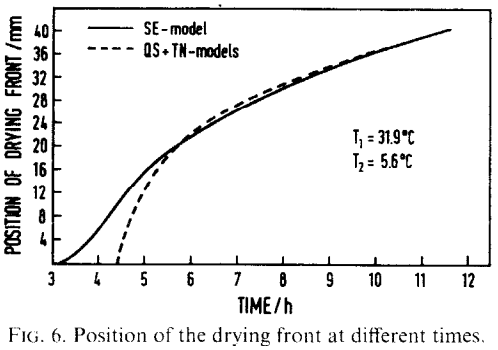


FIG. 6. Position of the drying front at different times.

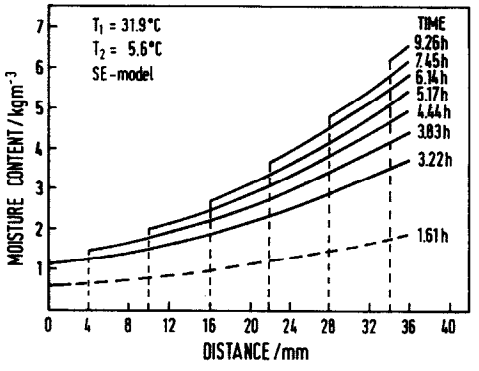


FIG. 7. Variation of liquid distribution in the slab with time.

mencement of drying. Again, it is seen that the QS and TN models predict a very rapid movement of the drying front, while the SE model shows a much slower movement.

Figure 7 shows the computed distribution of the liquid content within the slab during the drying process, using the SE model. It is seen that the liquid evaporated at the drying front is redeposited in the wet region of the slab, thus increasing the local liquid content. This increased liquid content causes the drying speed to drop as the drying front moves towards the cold face. The vapor reaching the cold face is condensed at this point. This quantity is not shown in the figure.

## CONCLUSION

Three models were considered for the analysis of transient moisture redistribution experiments with fiber glass slabs. The predictions of the QS model agree well with the results of the TN model. The overall trend of physical behavior predicted by the above models agrees with the experimental trends of variation. However, the predicted changes in the heat flux and the temperature distribution occur at a much faster rate than is observed experimentally. This observation lead to the development of an SE model based on the measured evaporation rate at the hot face. The evaporation rate is nearly constant during the initial quasi-steady period but decreases almost exponentially after the liquid content at the hot face has reached a critical value of about 25% of the fully saturated value. The inclusion of this 'falling rate' evaporation period in the SE model slows down the drying rate and thereby makes the agreement between the predictions and the experimental data much better.

## REFERENCES


1. M. Bomberg and C. J. Shirtliffe, Influence of moisture and moisture gradients on heat transfer thorough porous building materials, *Thermal Transmission of Insulations, ASTM STP* **660,** 211–233 (1978).
2. C. Langlais and S. Klarsfeld, Heat and mass transfer in fibrous insulations, *J. Thermal Insulation* **8,** 49–80 (1984).
3. W. C. Thomas, G. P. Bal and R. J. Onega, Heat and mass transfer in glass fiber insulating materials, *ASTM STP* **789,** 582–601 (1983).
4. M. K. Kumaran, Moisture transport through glass-fiber insulation in the presence of a thermal gradient, *J. Thermal Insulation* **10,** 243–255 (1987).
5. M. K. Kumaran, Comparisons of simultaneous heat and moisture transport through glass-fiber and spray-cellulose insulations, *J. Thermal Insulation* **12,** 6–16 (1988).
6. N. E. Wijeysundera, M. N. A. Hawlader and Y. T. Tan, Water vapour diffusion and condensation in fibrous insulations, *Int. J. Heat Mass Transfer* **32,** 1865–1878 (1989).
7. P. G. Crausse, G. Bacon and C. Langlais, Experimental and theoretical study of simultaneous heat and moisture transfer in a fibrous insulation, *J. Thermal Insulation* **9,** 46–67 (1985).
8. Y. Ogniewicz and C. L. Tien, Analysis of condensation in porous insulation, *Int. J. Heat Mass Transfer* **24,** 421–429 (1981).
9. S. Motakef and M. A. El-Masri, Simultaneous heat and mass transfer with phase change in a porous slab, *Int. J. Heat Mass Transfer* **29,** 1503–1512 (1986).
10. A. P. Shapiro and S. Motakef, Unsteady heat and mass transfer with phase change in porous slab, *Int. J. Heat Mass Transfer* **33,** 163–173 (1990).
11. K. Vafai and S. Whitaker, Simultaneous heat and mass transfer accompanied by phase change in porous insulation, *J. Heat Transfer* **108,** 132–140 (Feb. 1986)
12. K. Vafai and S. Sarkar, Condensation effects in a fibrous insulation slab, *J. Heat Transfer* **108,** 667–675 (Aug. 1986).
13. K. Vafai and H. C. Tien, A numerical investigation of phase change effects in porous materials, *Int. J. Heat Mass Transfer* **32,** 1261–1277 (1989).
14. H. C. Tien and K. Vafai, A synthesis of infiltration effects on an insulation matrix, *Int. J. Heat Mass Transfer* **33,** 1263–1280 (1990).
15. H. C. Tien and K. Vafai, Pressure stratification effects on multiphase transport across a vertical slot porous insulation, *J. Heat Transfer* **112,** 1022–1031 (Nov. 1990).
16. Y.-X. Tao, R. Besant and K. S. Rezkallah, Unsteady heat and mass transfer with phase changes in an insulation slab: frosting effects, *Int. J. Heat Mass Transfer* **34,** 1593–1603 (1991).
17. M. K. Kumaran and G. P. Mitalas, Analysis of simultaneous heat and moisture transfer through glass fiber insulation, *Proc. ASME/AIChE National Conf. on Heat Transfer*, HTD-78:1 (1987).
18. S. Hokoi and M. K. Kumaran, Experimental and analytical investigation of simultaneous heat and moisture transport through glass fiber insulations, *J. Thermal Insulation and Building Envelopes* **16,** 263–292 (1993).
19. Y. T. Tan, Effect of moisture on thermal insulation, M. Eng. Thesis, National University of Singapore (1989).
20. D. K. Edwards, D. E. Denny and A. F. Mills, *Transfer Processes*. McGraw-Hill, New York (1976).
21. S. V. Patankar, *Numerical Heat Transfer and Fluid Flow*. McGraw-Hill, New York (1980).
22. Chen Peishi and D. C. T. Pei, A mathematical model of drying processes, *Int. J. Heat Mass Transfer* **32,** 297–310 (1989).
23. M. Kaviany, *Principles of Heat Transfer in Porous Media*, p. 529. Springer, New York (1991).
24. O. A. Plumb, G. A. Spolek and B. A. Olmstead, Heat and mass transfer in wood during drying, *Int. J. Heat Mass Transfer* **28,** 1669–1678 (1985).
25. S. P. W. Wong and S. K. Wang, Fundamentals of simultaneous heat and moisture transfer between the building envelope and the conditioned space air, *ASHRAE Trans.* **96,** Part 2, 73–83 (1990).

## APPENDIX: QUASI-STEADY MODEL

For the quasi-steady period ($0 < t < \tau_s$), the heat flux and the temperature distribution were obtained in ref. [6]. These can be written as:

$$q_0(z) = \frac{k_0[T_1 - T_2]}{L} + H_{fg}\rho_a D_0 \frac{[g(T_1) - g(T_2)]}{L} \quad \text{(A1)}$$

$$k_0(T - T_1) + H_{fg}\rho_a D_0[g(T) - g(T_1)] = k_0 \frac{(T_1 - T_2)z}{L} + H_{fg}\rho_a D_0 \frac{[g(T_1) - g(T_2]z}{L}. \quad \text{(A2)}$$

After the onset of the dry-out at the hot surface, $z = 0$, there will be a dry region and a wet region in the slab. When the drying front has reached a distance $x$ from the hot surface, the heat flux is obtained by solving the energy equation in the wet region. This is given by

$$q(t) = \frac{k_0(T_3 - T_2)}{(L - x)} + H_{fg}\rho_a D_0 \frac{[g(T_3) - g(T_2)]}{(L - x)}, \quad \text{(A3)}$$

where $T_3$ is the temperature of the wet–dry interface.

The temperature $T_3$ is obtained from the solution of the equation:

$$q_d(L - x) + k_0(T_2 - T_3) + H_{fg}\rho_a D_0[g(T_2) - g(T_3)] = 0, \quad \text{(A4)}$$

where $q_d$ is the heat flux in the dry region.

The temperature distribution in the wet region, $T_w(z)$, is given by

$$k_0 T_w + H_{fg}\rho_a D_0 g(T_w) = k_0 T_2 + H_{fg}\rho_a D_0 g(T_2) + \left[\frac{L - z}{L - x}\right]\left[k_0(T_3 - T_2) + H_{fg}\rho_a D_0[g(T_3) - g(T_2)]\right]. \quad \text{(A5)}$$

The condensation rate $\Gamma$ at the point $z$ in the wet region is given by the expression

$$\Gamma(z) = \frac{k_0}{H_{fg}}\left[\frac{q_d H_{fg}\rho_a D_0 g''(T_w)}{[k + H_{fg}\rho_a D_0 g'(T_w)]^3}\right]. \quad \text{(A6)}$$

The liquid saturation is obtained by substituting in equation (2). This gives

$$\frac{\partial\theta}{\partial t} = \frac{\Gamma(z)}{\varepsilon\rho_w}. \quad \text{(A7)}$$

The rate at which the drying front moves is given by the mass balance at the wet–dry interface as

$$-\varepsilon\rho_w\theta(x, t)\frac{dx}{dt} = \frac{H_{fg}\rho_a D_0 g'(T_3)}{k_0 + H_{fg}\rho_a D_0 g'(T_3)}. \quad \text{(A8)}$$

The quasi-steady expressions (A5) and (A6) are used to compute the temperature distribution and the condensation rate distribution in the wet region. The change in the liquid saturation during a small time $\Delta t$ is obtained from equation (A7). Equation (A8) gives the distance $\Delta x$ that the drying front moves during the time $\Delta t$. For the new position of the drying front $(x + \Delta x)$, the quasi-steady expressions (A3) and (A4) are used to compute the heat flux and the temperature at the wet–dry interface, respectively. The procedure is continued until the drying front reaches the cold face of the slab.

The effect of the heat-flux-meters are accounted for by a simple iterative procedure. The heat flux is first computed by assuming zero thermal resistance of the heat-flux-meters. This heat flux and the known thermal resistance of the heat-flux-meters (0.015 $m^2$ K $W^{-1}$) is used to compute the temperature drop across the heat-flux-meters. The new temperatures at the hot and cold faces of the insulation are used to obtain a more accurate heat flux using expression (A3). This procedure converges within about four iterations.